2022

Apparatus Improvement and Characterisation for Experiments on Ultra-cold Plasmas.

Jakub Bystrický

Apparatus Improvement and Characterisation for Experiments on Ultra-cold Plasmas.

Jakub Bystrický

An Honours Thesis presented to the faculty of the

Department of Physics and Astronomy at

Colby College

Department of Physics and Astronomy

Colby College

Waterville, ME

May, 2022

Abstract

Plasmas are the most common state of ordinary matter in the universe [1]. They exist over wide temperature and ion density ranges. One of the types of plasmas is Ultra-cold neutral plasmas (UNPs). These are created by laser cooling atoms in a magneto-optical trap and successive ionisation. They are of interest to many researchers as they allow us to study plasma dynamics without extremely high temperatures and they can exist in a strongly coupled regime in a laboratory.

In this thesis, the apparatus for creating UNPs was improved and data on plasma expansion was collected. We increase the trapping efficiency of a quadrupole magneto-optical trap (MOT) by installing a tapered amplifier to increase the power of the cooling laser used to trap atoms. We achieve an improvement in density of trapped atoms from $\sim 1 \times 10^{10}\ \mathrm{cm}^{-3}$ to $\sim 2.5 - 4.5 \times 10^{10}\ \mathrm{cm}^{-3}$. In addition, to improve precision and decrease systematic error, the magnetic field induced by inductive current in the MOT's anti-helmholtz coils was suppressed. This was achieved by installing a KEPCO Bipolar Power Supply ($\pm 36\ \mathrm{V}$), which allowed for suppression of induced current to sub $200\ \mu\mathrm{A}$ magnitudes during the experiment.

Expansion velocity of an ultra-cold neutral plasma was studied using ion time of flight (TOF) spectra collected for a rubidium plasma with initial electron temperatures of $1 - 150\ \mathrm{K}$ and initial ion temperatures of $< 100\ \mu\mathrm{K}$. We predicted a constant expansion velocity for a given initial electron temperature and our data generally agrees with this prediction well. However, for low initial electron temperatures and early in the plasma evolution we see a non-linear region. We suspect this is a result of the effects of three-body recombination. As such, we demonstrate that using ion TOF is a good way for studying spatial evolution of UNPs.

Acknowledgments

I would like to express my deepest gratitude to Professor Duncan Tate as without his willingness to supervise and support me throughout the process, I would not be able to complete this thesis. Professor Tate allowed me to join his laboratory in my sophomore year and had guided me since then to be a better researcher and a better physicist. I am extremely thankful for all the trust and time he has given to me throughout my time at Colby College.

Furthermore, I would like to appreciate Professor Charles Conover's willingness to help, especially when we struggled with the installation of the new power supply. I also wish to share my gratefulness to Professor Robert Bluhm - who helped me with my graduate school applications, Professor Jonathan McCoy - who helped inspire and convince me to choose the physics major, Lisa Lessard - who hired me as a laboratory teaching assistant, and the entire Physics Department of Colby College, which was my home away from home for four years.

I would like to acknowledge the work of Changling Li and Coulson Zhi, who worked in Prof. Tate's lab at different times during my time at Colby. I would also like to acknowledge Huan Bui, who allowed me to use his Latex formatting for this thesis. Alongside them, I would like to share my thanks with all my fellow physics majors, whom I spent many long nights with fighting our way through problem sets. I would not be able to complete this thesis without the support of my parents - Alena and Erik, my closest friends - Lutie, Katie, Eileen, Iliana, Yeeun, Akezhan, and my girlfriend - Auroshree.

Lastly, I wish to give special thanks to Professor Thamattoor for letting me work in his organic chemistry laboratory in my first year, which allowed me to gain valuable experience as a researcher. My thanks also go to Ed - for being willing to hire me as his laboratory teaching assistant, Sue and Masi - for overseeing the international students program at Colby, and Dan - for support and guidance. Without all these people, and many more, my time at Colby would not be enjoyable and I would not choose to write this thesis. Thank you!

Contents

Chapter 1

Introduction

1.1 Plasma

Plasma is the fourth and most common state of ordinary matter in the universe. In fact, around 99% of all matter in the universe is in the plasma state [1]. Plasma is an ionised gas that exhibits collective behaviour. The electromagnetic forces between the electrons and the ions cause the collective effects. Star coronas and stars are an example of plasmas in space, but there are a few examples of plasmas on earth too. Namely, lightning bolts are a plasma all of us have seen. Another example is plasmas that form in the ionosphere due to incoming solar radiation. Plasmas can exist over a wide range of electron and ion temperatures and densities. Star coronas have several thousands degrees Kelvin, while the ionosphere plasmas do not cross a few hundreds degrees Kelvin [2]. Thus, what makes an ionised gas a plasma must depend on more than just the temperature of the ionised gas. It is, in fact, the density of the charged particles that plays the role. The ionosphere plasmas have a density of $10^3\ \mathrm{cm}^{-3}$ while the center of the sun has plasma densities on the order of $10^{27}\ \mathrm{cm}^{-3}$ [2]. Therefore the two main characterisations of plasmas will be their temperature and their electron and ion number densities.

When the density is high enough and the temperature low enough the particles can get so close to each other that the energy coming from the Coulomb forces is equal or larger than their thermal (kinetic) energy. This is captured by the Coulomb coupling parameter Γ. This coupling parameter can be specified for both ions and electrons and it is given by [3]:

$$\Gamma = \frac{E_{interaction}}{E_{thermal}} = \frac{e^2}{4\pi\epsilon_0 a k_B T} \tag{1.1}$$

where all the known constant are as usual and $a = \frac{3}{4\pi n}^{1/3}$, n being the number density, is the mean separation of electrons or ions, known as the Wigner-Seitz radius. A plasma is said to be strongly coupled when $\Gamma \geq 1$ and weakly coupled when $\Gamma < 1$. Note the fact that electrons are strongly coupled ($\Gamma_e \geq 1$) does not imply that the ions are strongly coupled too and vice versa. Most of the naturally occurring plasmas are weakly coupled due to large spacing between atoms, but there is some plasmas that can be strongly coupled (see **Figure 1.1**).

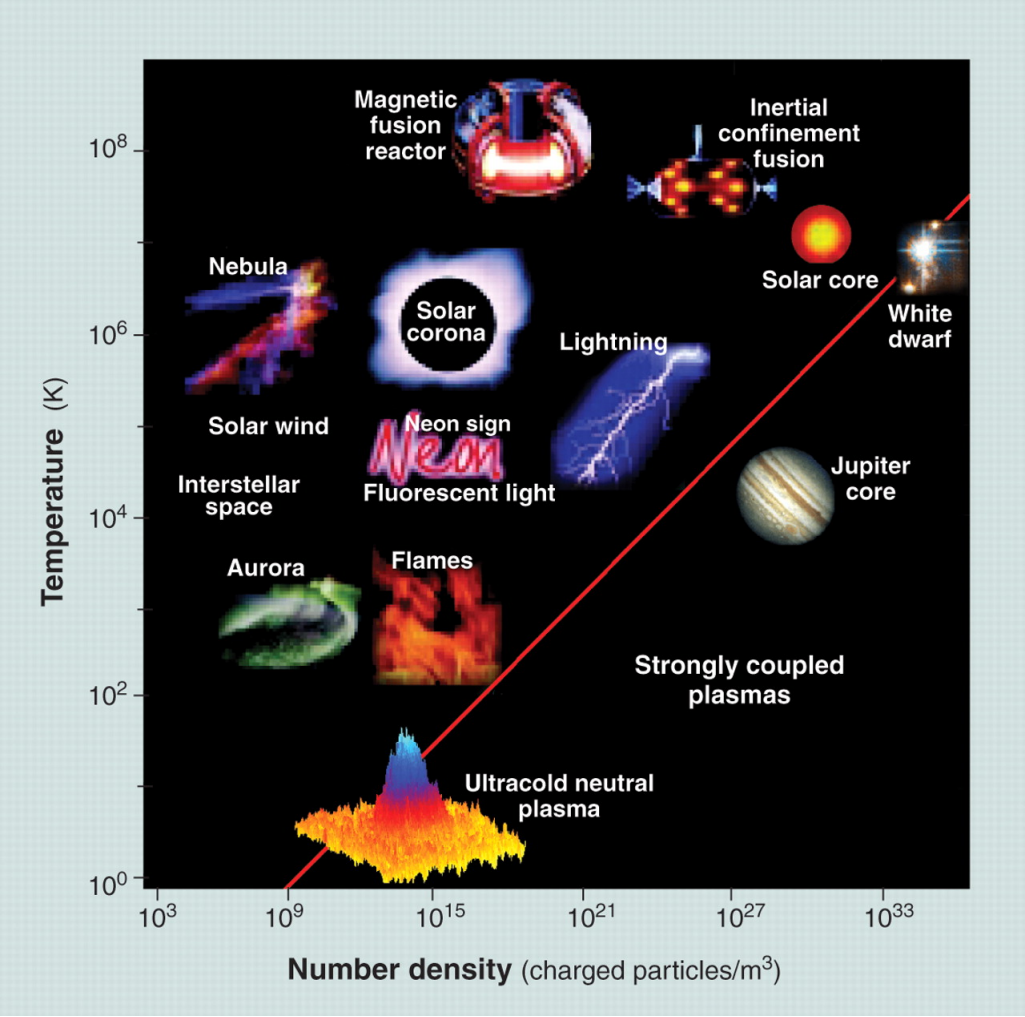

Figure 1.1: Examples of plasmas occurring naturally as well as laboratory created plasmas. The red line represents the split between strongly and weakly coupled plasmas ($\Gamma = 1$) [4].

1.2 Ultra-cold Neutral Plasmas

Despite the fact that most plasmas are very hot and have large amounts of energy, it is possible to create a plasma that is ultracold. The first ultracold neutral plasma (UNP) was created in 1999 by Steve Rolston's group at NIST [1]. This UNP was created by ionising Xenon atoms that were cooled and trapped using a magneto-optical trap (MOT).

Even though the first UNP was created using Xenon, UNPs can be created from almost any atom that can be laser cooled, trapped, and ionised relatively easily. A very common choice is alkali metals and alkali earth metals. The alkali metals are a little easier to trap and cool, as they have an easily accessible valence electron and a single transition cooling cycle. On the other hand, alkali earth metals have the advantage of having optical transitions in ions, which allow for direct optical measurements. For experiments in this thesis we use natural rubidium , which is around 28% Rb-87, and the rest is Rb-85 [5].

Since 1999, much of the research on these new plasmas was motivated by the possibility of reaching the strongly coupled regime, which is extremely rare in commonly occurring plasmas. Once a plasma is in this strongly coupled regime, it starts acting very differently. Namely, it can start exhibiting liquid or even solid like properties. These occur when $1 < \Gamma \leq 170$ and $\Gamma > 170$ respectively [6]. UNPs are a great candidate for a strongly coupled plasma regime due to their low energy, much higher ion densities can be achieved. The ability to influence the initial density by control of the ionising beam and the cooling system gives physicists great control over the evolution of the plasma.

Though some strongly coupled UNPs have been created, they did not exceed $\Gamma = 3$ [7–9]. This is due to inherent limitations that come from the fact these plasmas form at really low temperatures; the initial ion temperatures are usually on the μK scale. Why these low temperatures create a limitation will be explained in the coming sections.

1.3 Creation of UNPs

We have mentioned earlier that UNPs can be created by trapping atoms in a MOT and subsequently photoionising them. A key aspect of atom trapping is the ability to laser cool atoms. This

method was developed by Steven Chu, Claude Cohen-Tannoudji, and William D. Phillips and in 1997 they received a shared Nobel prize for it [10]. We can optically cool atoms by shining lasers at a cloud of atoms from 6 opposing directions.

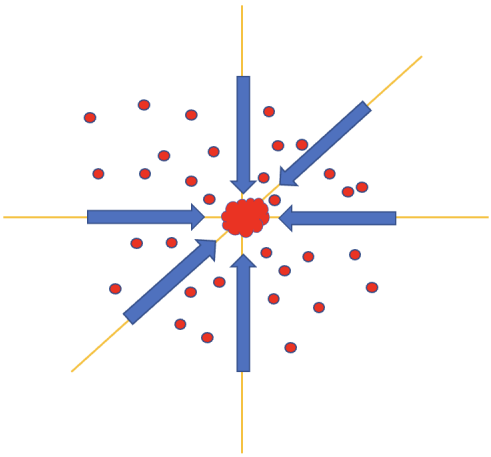

Figure 1.2: Laser cooling using six cooling laser beams. The atoms slow down by losing their momentum from absorbing and re-emitting photons coming from lasers opposing the atoms' path.

These lasers are frequency calibrated to match a transition in the trapped atom so that when it absorbs the photon it loses some of its momentum. This, however, does not work when the lasers are set exactly to the wavelength needed for the excitation because of the Doppler shift experienced by the atoms. This *issue* turns out to be the key to the success of laser cooling. Due to the Doppler shift, the energies required to excite an atom traveling towards and away from a laser are different. As such, the lasers are detuned so that only atoms traveling in opposite direction to the beam absorb the photon and lose some of their momentum in that direction. Since this slowing happens in all six directions (see **Figure 1.2**), we slowly decrease the atom's momentum overall. There is a limitation to this process though, as eventually the atoms slow down enough so that the Doppler shift is no longer significant, which is the cooling limit of the trap. This can be avoided by adjusting the detuning with time, but is usually not an obstacle as even without that, temperatures of the μK order can be reached with no issues. It is important to mention that there is multiple ways lasers can be configured to cool atoms, this is the one presented as it is the one used in the experiments in this thesis.

Thus far we described how lasers can cool atoms. However, these atoms must be confined to

a small region, otherwise the likeliness of the atom crossing the path of any of the lasers is very low. This is where the magnetic part of the MOT is relevant. The arrangement of the magnetic field inside the trap can vary greatly, just like the arrangement of lasers. However, no matter the trap configuration, the magnetic field is set up so that it always leads atoms back to the region where they can be cooled. The trap used in this thesis is a quadrupole trap. The magnetic dipole of Rubidium interacts with the field which always leads the molecules into the centre of the trap.

As the atoms cool and group in the middle of the trap, we can apply an ionising beam, usually coming from a pulsed laser. This pulse creates ions and electrons which together form the plasma. The kinetic energy of the electrons is the excess energy of the pulse laser, compared to required ionisation energy. This process is also described in **Figure 2.3**.

Using the MOT we can create very dense samples of cold atoms. As such, the ion densities after ionisation will also be very high, which is necessary if one hopes to create a strongly coupled plasma. The number density of the cold atoms and thus also ions in the plasma (i.e. at times after the ionisation) is Gaussian and is given by [11]:

$$n_i(r,t) = \frac{N_i}{(2\pi\sigma^2)^{3/2}} e^{-r^2/2\sigma^2} \tag{1.2}$$

where N_i is the number of trapped atoms and σ is the characteristic width of the Gaussian distribution. The number density depends on the number of trapped and cooled atoms. We can therefore increase the density by increasing the cooling power of the trap. This is one of the goals of the first part of this thesis.

The ionising beam creates photoions, but because of the great mass difference between the electron and the ion, most of the excess energy from the ionising photon is given to the electron. That is, the electrons are hot compared to the rest of the now ionised cloud. Due to the high kinetic energy, a portion of these electrons escapes immediately from the cloud. The remaining system is no longer neutral and thus forms a potential well that prevents remaining electrons from escaping. It is still mostly neutral, though. At a certain point, enough electrons escape so that the potential well of the now positive ion cloud is deep enough to prevent the remaining electrons from escaping (see **Figure 1.3**). This allows the collective behaviour of the cloud and thus is the moment of plasma creation.

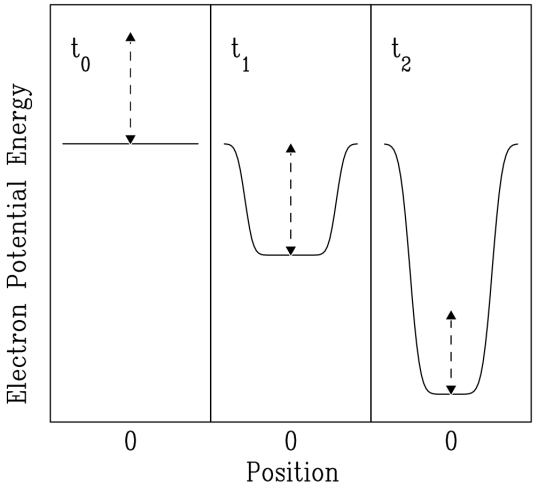

Figure 1.3: Potential well depth (solid line) vs. the energy of an electron (dashed line) at different times. The later the time, the more electrons have escaped the plasma. Figure from "Creation of an Ultracold Plasma", 1999 [1].

1.4 Basic UNP Dynamics

1.4.1 Expansion

Since the cloud is slightly positive the ions feel Coulomb forces and the cloud starts expanding. Another factor that affects the expansion is the electron pressure within the cloud, which increases with increasing electron temperature. Thus, higher initial electron temperatures mean faster expansion and shorter plasma lifetime. As the UNP expands, the depth of the potential well decreases and even though expansion cools electrons adiabatically, more electrons start escaping, leaving the plasma even more positive. This process is what, in the end, determines the achievable lifetime of the plasma, which is usually less than $100\ \mu$s. The velocity of this expansion is assumed to be uniform and to be given by [12]:

$$v_0 = \sqrt{\frac{k_B(T_{e,0} + T_{i,0})}{m_{ion}}} \tag{1.3}$$

where the $T_{e,0}, T_{i,0}$ are the initial temperatures of electrons and ions, respectively. The expansion velocity was first measured by S.Kulin in 2000 [13]. Measuring the expansion velocity of a rubidium plasma is the purpose of the experimental section of this thesis. For the measurements to accurately describe the expansion we must eliminate the magnetic fields of the trap for the

duration of plasma lifetime. The reason is that if the magnetic field is still on, then the ions and electron trajectories will be affected by the fields. These effects can be significant enough to interfere or change the collective behaviours of the plasma and so eliminating the magnetic field is another goal of this thesis.

1.4.2 Heating and Cooling Processes

It is important to note that when we say the plasma temperature changed we mean the temperature of either ions or electrons (or both) changed. The behaviour of the overall plasma tends to depend on the temperature of electrons more - at least for the purposes of this thesis. This is because the electron kinetic energy is orders of magnitude larger than the ion temperature. As such, a slight change in ion temperature is not as significant as a same relative change in electron temperature.

There are several heating and cooling processes that happen in the plasma. One cooling process is the expansion itself, via which the plasma cools adiabatically. Disorder induced heating is one of the processes that affects the temperature of the ions. Namely, after some electrons escape, the ions organise themselves in a more regular pattern as that decreases their potential energy and thus by conservation of energy their kinetic energy must increase.

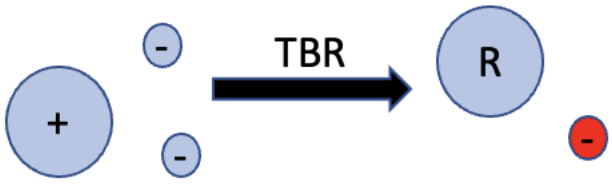

Figure 1.4: Three body recombination process. On the left hand side: two cold electrons and a cold ion. On the right hand side: A cold Rydberg atom and a hot electron. The electron is hot as it inherits the energy released by combining the cold electron and ion.

Another heating process for electrons is three-body recombination (TBR). In this recombination an ion and two electrons collide to form a cold Rydberg atom and a hot electron, as depicted in **Figure 1.4**. The electron heats up by absorbing the energy released when the other electron

combines with the ion to form the Rydberg atom. As this requires low energy electrons, ions, and a high enough density it is a process that only happens with significant frequency early in the plasma evolution and only for low initial electron temperatures. This is the process that limits UNPs from easily reaching the strongly coupled regime as conditions that make TBR more frequent are exactly the ones required for strong coupling. It has been a long-term goal of the Tate Laboratory at Colby College to create a strongly coupled UNP by trying to combat TBR by seeding the plasma with cold Rydberg atoms used as ”ice-cubes”. This would be done by a second pulse laser (in addition to an ionising laser) that would excite a portion of the cloud into Rydberg states.

Chapter 2

Apparatus and Improvements

The general setup for the creation of the plasma can be divided into three sections: the MOT, the cooling lasers, and the ionisation lasers. We will consider all these sections and describe the setup. Most of the setup was built by Prof. Tate and his previous students and the theses they wrote have been consulted in writing of this chapter. As part of this honors thesis, a few improvements were made on the setup. In particular, a tapered amplifier was installed to increase the cooling power and a better elimination of the magnetic field in the trap during plasma lifetime was achieved by a new power switching mechanism.

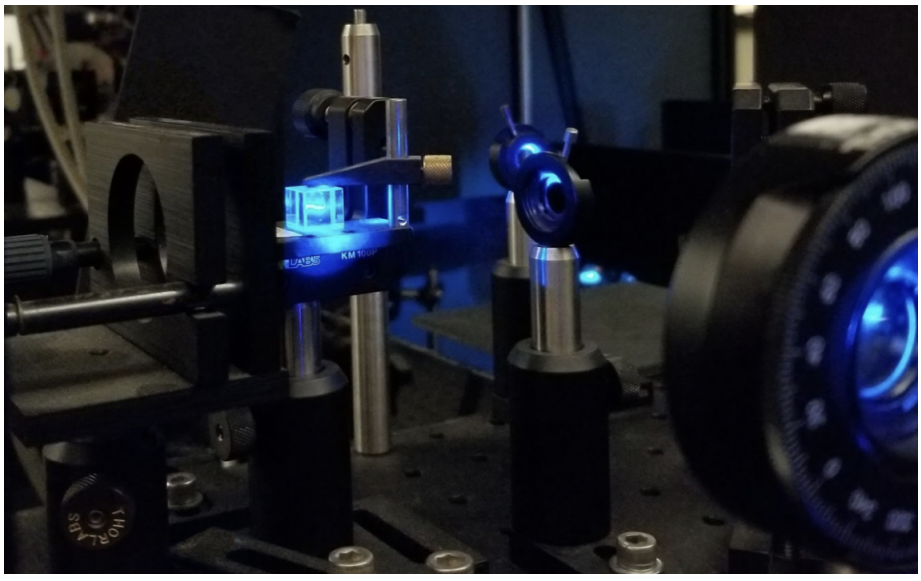

Figure 2.1: A beam splitter illuminated by a beam from a Littman dye laser used to ionise cooled Rubidium atoms.

2.1 MOT

The vacuum chamber part of the MOT used in this thesis was built by Prof. Duncan Tate. It is a stainless steel vacuum chamber with an ion pump and a connected Rubidium finger valve. The chamber has 6 windows to let the cooling lasers enter, see **Figure 2.2** and a window for the ionising laser too. To keep the atoms centred in the middle of the trap, a quadrupole magnetic field is created using copper wires coiled around the trap (anti-Helmholtz configuration). There is a set of field meshes and an MCP detector inside the vacuum chamber, which is used to detect the UNP.

The pressure in the trap is as low as 10^{-10} Torr [11] and the maximum atom density achievable is 5×10^{10} cm^{-3}. However, we do not usually create a plasma from a cloud of this maximum density. One of the reasons for why we do not use this maximum density clouds is that with increasing cooling power both the size and density of the cold atom cloud increase, but the setup inside the trap only allows for reliably observing clouds of radius < 9.5 mm (see **Section 2.3**. The temperatures of cold atoms in the trap are ~ 100 μK.

The cloud inside the trap is monitored by a CCD camera that is pointed at the cloud through one of the windows. Through yet another window a Coherent power meter measures the fluorescence of the cloud of atoms. These two measuring methods are used when determining the clouds density and size. The readings on these have to be done manually and thus these methods are not useful during plasma experiments where the observed phenomena happens on microseconds scale.

2.2 Laser Cooling

The preparation of cold Rubidium atoms is key in the process of creating the plasma. The setup of the laser beams and optical devices is shown in **Figure** 2.2.

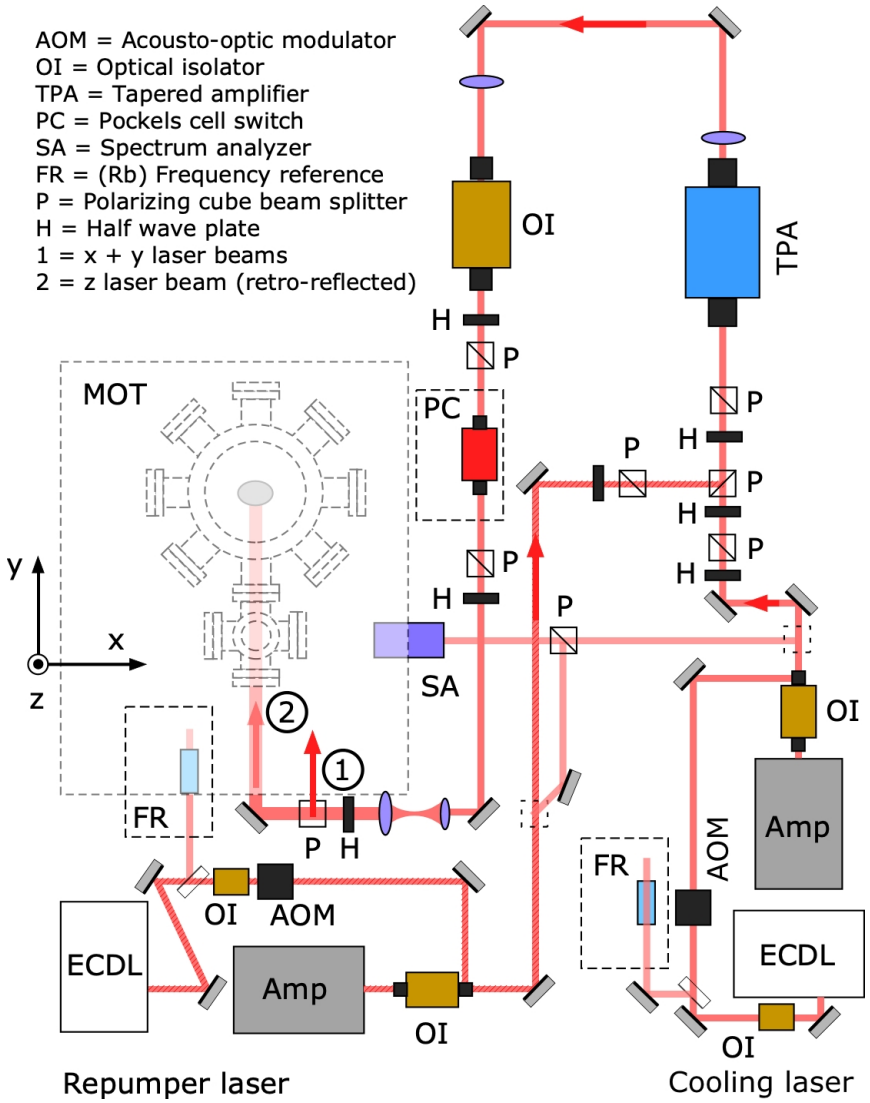

Figure 2.2: Setup of the laser cooling system, mostly built by Prof. Tate and his previous students. As part of this thesis the TPA and the Pockels cell with its adjacent optical isolator were installed. The diagram was used with permission of Prof. Tate.

The cooling transition in Rb-85 is $5s_{1/2}\ F = 3 \longrightarrow 5p_{3/2}\ F' = 4$. Most atoms will decay from the $5p_{3/2}\ F' = 4$ state back to the $5s_{1/2}F = 3$ state and thus stay in the cooling cycle. However, a few of them will fall into the dark state, which is the $5s_{1/2}\ F = 2$ state. To recover these atoms a shorter wavelength light is required, which comes from the repump laser. Unless the repump laser is running the cooling efficiency is minimal, as eventually all atoms end up optically pumped to the dark state and there can be no more cooling.

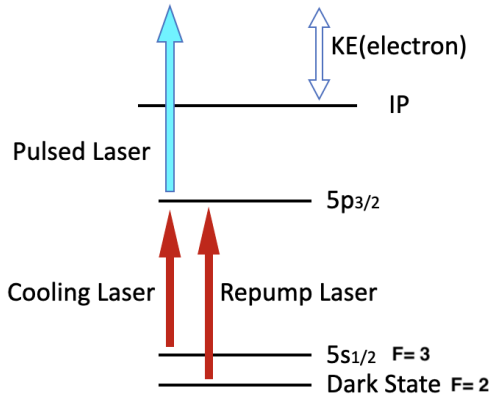

Figure 2.3: The cooling transitions are in red, where most atoms decay to the $5s_{1/2}$, $F = 3$ state and only some fall to the dark state; $F = 2$. The pulse laser ionises the excited atoms past their ionisation potential (IP) and gives the freed electron the kinetic energy equal to the excess photon energy.

Both the cooling and the repump lasers are continuous wave diode lasers. Generally, the bandwidth of diode lasers is too large to single out one cooling transition. For this reason, an external cavity is used. A diffraction grating provides a first order diffracted beam as the optical feedback to the diode. The lasers are frequency stabilised and tuned using frequency reference rubidium cells. In these cells rubidium gets excited to the $5p_{3/2}$ $F' = 4$ state and spontaneously decays to the ground state. The Doppler-free wavelength of the emitted photons is the wavelength needed for the transition. The cooling lasers are locked to this frequency - detuned by $10 - 20$ MHz to account for Doppler shifts experienced by room temperature atoms, so that only atoms travelling in the direction opposite to the beam can accept the photons. The actual wavelength of the cooling laser is 780 nm. To lock both the cooling lasers, laser locking boxes are used, which control the wavelengths by applying voltage to a piezoelectric element that controls the diffraction grating in the external cavity of the lasers.

The laser beams from the cooling laser and repump laser are aligned and travel towards the vacuum chamber together, see **Figure 2.2**. After initial amplification of the beams, the aligned beam had power of $10 - 20$ mW. The tapered amplifier increases the joint laser power to ~ 350 mW. The optical switch shown in the **Figure 2.2** is not currently in use, but was installed with the intention to eliminate the effect of the cooling lasers on the expanding plasma by preventing them from entering the trap for the duration of the measurement. The joint beam enters the chamber

from three sides and is then back reflected so that the cooling occurs from six directions. Right before entering the trap, two lenses are used to expand the joint beam to increase the interaction region.

2.3 Ionisation

The cooled atoms get ionised by a pulsed laser. This laser uses 3rd harmonic of an Nd:YAG laser ($355\ \mathrm{nm}$) as an energy source for a Littman-configuration dye laser [14]. The repetition rate of the laser is $20\ \mathrm{MHz}$ and the pulse duration is $\sim 5\ \mathrm{ns}$ [15]. The dye used is Coumarin 480 dissolved in methanol. This dye's peak emission occurs at $\sim 473\ \mathrm{nm}$ [16]. The ionisation wavelength required for Rubidium 85 in its $5p_{3/2}$ state is $479\ \mathrm{nm}$. The energy difference between the ionisation energy and the photon energy is absorbed by the freed electron and determines its initial temperature, see **Figure 2.3**. The wavelengths used are in the range $475 - 479\ \mathrm{nm}$, corresponding to $0 - 150\ \mathrm{K}$ initial electron temperatures, $T_{e,i}$. The wavelength of the laser is controlled by a diffraction grating, where an analog dial measures its angle. The Littman laser was calibrated using a spectrometer so that we know exactly what dial setting corresponds to what wavelength, and thus to what initial ion temperature. In particular, the table below shows what dial settings (in degrees, minutes, and seconds) are required for different initial electron temperatures that were determined during the calibration of the laser.

$T_{e,i}$	λ_{vacuum}	Degrees	Minutes	Seconds
1K	479.035	310	42	5
10K	478.820	310	45	23
20K	478.581	310	48	42
30K	478.342	310	52	1
50K	477.866	310	58	38
70K	477.390	311	5	15
100K	476.678	311	15	11
150K	475.497	311	31	44

Table 2.1: This table shows the initial electron temperatures ($T_{e,i}$) and the corresponding ionisation Littman laser beam wavelengths required to achieve these temperatures. The other three columns refer to settings on an analog dial that is used to set the Littman laser wavelength. However, the smallest division on the dial is a minute, thus the seconds cannot be reliably accounted for.

2.4 Ion TOF - Detection of the UNP

To detect the expansion rate of the plasma we use ion time of flight (TOF) spectra. Once the plasma is created its ions are (assumed to be) in a Gaussian distribution. At a chosen time, we can apply an electric field which pushes them towards the micro-channel plate (MCP) detector. This field is created by applying a high voltage (HV) pulse to the field meshes inside the trap. These are $d = 19$ mm apart and thus we see where the atom cloud radius size limit of 9.5 mm comes from. The distance from the meshes to the MCP is $l = 38$ mm. The high voltage pulse is short rise time (< 10 ns) and creates an electric field of < 200 Vcm^{-1}during the measurement. It has a duration of 1 μs.

Important to note is that once the HV pulse is applied, electrons leave the cloud much faster than the ions due to their lower mass. As such, there is a moment when the plasma is almost entirely positive and starts expanding rapidly due to Coulomb forces between the ions. We have not checked for how significant this effect is on the results.

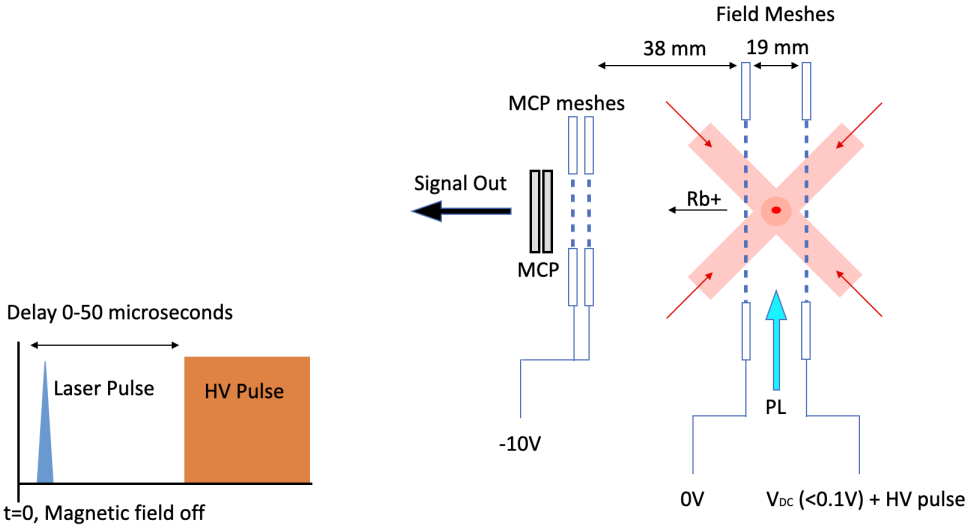

Figure 2.4: Right: The setup of the inside of the MOT used to detect and study the plasma. PL = pulse Laser. The red arrows represent the cooling lasers. Left: Scheme of the timing and delays of the laser and HV pulse.

Different ions will be in different places and their travel time to the MCP detector will be different. As such, we can infer their position from the ion TOF acquired. By acquiring the ion TOF at different times in the plasma evolution we can get a picture of the spatial evolution of the

plasma over time. When we say at different times, we mean at different times after the ionisation of the atom cloud. A diagram illustrating the timing of the HV pulse is shown in **Figure 2.4**. The delays are controlled by four delay generators (three DG535's and a DG645 - all from Stanford Research Systems, Inc.). The delay between the magnetic field turning off and ionisation laser pulse is kept constant at $50\ \mu$s. The delay between the pulse of the laser and the HV is what we change in order to study the expansion. The usual delay ranges between the laser pulse and the HV pulse are between $0.5\ \mu$s and $35\ \mu$s.

2.5 Tapered Amplifier (TPA)

As part of this thesis a tapered amplifier was installed. The reason for the installation of this amplifier was increasing the cooling power of the trap by increasing the laser power (and thus the number of photons). Greater cooling power leads to a greater number of cooled atoms. This translates to both a larger cloud and a denser sample.

The amplifier itself was built by Ryan Cole, Phd as part of his honors thesis. The overview of the amplifier's structure is shown in **Figure 2.5**. The aspherical lenses focus the beam into the TA crystal and then expand it to its original size. TA chips have two basic sections: waveguide and then the gain medium. The waveguide is narrow ($3\ \mu$m) tube that leads the beam to the gain medium, hence the focusing that is required. The gain medium has a tapered shape and via diffraction, the beam fills the entirety of the gain medium. The medium is uniformly pumped by an adjustable current [17], which affects the output.

To install this amplifier a few polarising beam splitters and polarisers had to be added to the setup as the TPA can only accept light of a single polarisation - in our case it is set up to be horizontal. We also had to ensure limited back reflection from further down in the setup (to not damage the TA chip) - by means of an optical isolator.

The actual setup is shown in **Figure 2.2**. The power output of the amplifier, for a seed beam of $\sim 10 - 20$ mW is ~ 350 mW at an operational current of ~ 1.1 A. The usual density of the trapped ions before the installation of the TPA was $\sim 1 \times 10^{10}\ \mathrm{cm}^{-3}$ [17]. To evaluate the efficiency of the TPA we recorded the size and density of the atom cloud for different operational currents (see **Table 2.2**).

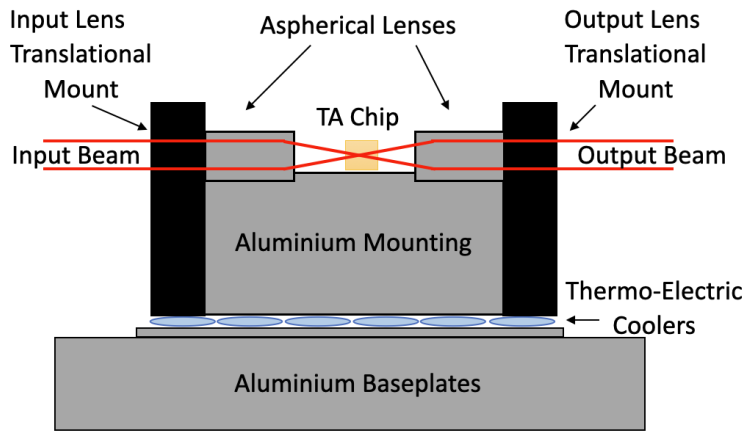

Figure 2.5: Tapered amplifier design. This amplifier was built by Ryan Cole, PhD as his undergraduate honors thesis - and the diagram was made to reflect his diagram.

TPACurrent (A)	FWHM (μs)	σ (cm)	N	n (cm^{-3})
1.1	650	4.6×10^{-2}	1.1×10^{8}	2.5×10^{10}
1.2	550	3.9×10^{-2}	1.2×10^{8}	4.5×10^{10}
1.3	700	5×10^{-2}	1.7×10^{8}	3.1×10^{10}
1.4	700	5×10^{-2}	1.8×10^{8}	3.2×10^{10}

Table 2.2: Supply current to the TPA and the atom density achieved for input beams of $\sim 10 - 20$ mW power. n is density, N is number of atoms, $FWHM$ is the width of the signal received from a linear array diode, and σ is the characteristic width of the atom cloud.

To determine the values listed in **Table 2.2** we collected the fluorescence power of the trapped atoms using a Coherent power meter at the focus of $d = 45$ mm diameter lens. The power captures a fraction of the emitted light, following the relationship below:

$$P = \frac{N}{2} h\nu \frac{\pi d^2}{16\pi l^2} \frac{1}{\tau} \tag{2.1}$$

where h is Planck's constant, $\nu = (c/780.24)$ nm is the frequency of the emitted photon, $\tau = 27$ ns is the lifetime of the $5p_{3/2}$ state, and $l = 190$ mm is the distance from the cold atoms to the lens. N is divided by two as only half of the atoms are in the excited state at saturation. This gives us a way to find the number of atoms in the trap N.

To determine the radius of the cloud, we first find the FWHM of the atom cloud fluorescence

using a linear array diode and an oscilloscope, which is a measurement in the units of time. The diode has length $L = 28.7\ \mathrm{mm}$ and it downloads CCD pixels in $T_L = 12.5\ \mathrm{ms}$. As such we have the following relationship:

$$\Delta x = \frac{\Delta t}{m T_L} \Delta t \tag{2.2}$$

where $m = 1.2 \pm 0.1$ is the linear magnification of the imagining system. We can now use this finding to determine σ, the characteristic width of the Gaussian distribution we assume the cloud to have. The relationship between this Δx and σ is given by:

$$\Delta x = 2\sqrt{2 \ln 2}\sigma \tag{2.3}$$

At this point we have all the information necessary to calculate the cloud's density as shown in **Equation 1.2**. However, we are interested in the average density, which we can find by integrating as follows:

$$\overline{n} = \int_0^\infty n(r) n(r) 4\pi r^2 dr = \frac{N}{(4\pi\sigma^2)^{3/2}} \tag{2.4}$$

Using the process above, we acquired the values listed in **Table 2.2**. The trend agrees with the calibrations done with this TPA earlier (in Ryan Cole's thesis) [17]. The reason for which the density starts dropping is that for densities that are too high, the atoms start pushing away from each other due to the clouds internal pressure.

We can see that the operational current that is most efficient is $1.2\ \mathrm{A}$. However, due to the limited size of the trapping region, the usual current applied to the TPA during experiments is $\sim 1\ \mathrm{A}$. The measurements above were repeated multiple times with very similar results.

2.6 Reducing Induced Magnetic Fields

To study the natural expansion of the plasma we must minimize background magnetic fields, as they would affect the behaviour of the ions in the plasma. In prior experiments the power supply used to power the MOT anti-Helmholtz coils could only produce positive voltages. As such, to

limit the magnetic field the power supply of the anti-Helmholtz coils was simply turned off for the duration of plasma lifetime. However, due to the inductance of the wires, there was still magnetic field present in the trap. As a part of my thesis, this issue was significantly eliminated. The issue was solved by:

a) installing a new power supply that can switch between positive and negative voltages (with a greater output magnitude range too)
b) by calculating and developing a new power switch control

The power supply installed is a KEPCO Bipolar Power Supply with a range ± 36 V and it is controlled by a Tektronix AFG3022 function generator. The final waveform as it is calculated below was written using ArbExpress, a Tektronix utility program to control the AFG3022, and then transferred to the function generator.

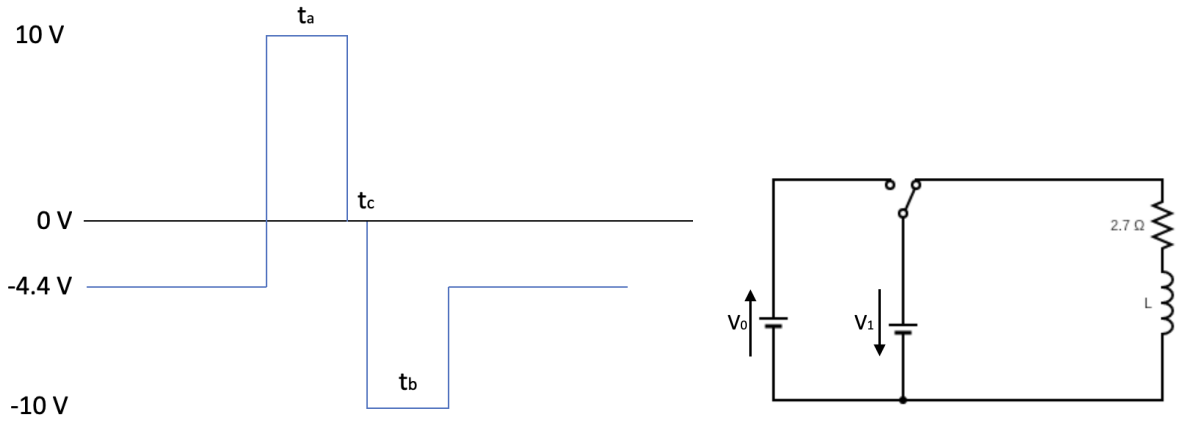

Figure 2.6: Left: The waveform generated by AFG3022 that controls the power supply to the coils. The current during trapping is ~ 6 A, which corresponds to a 16 V voltage across the wires and a ~ -4.4 V output from the AFG3022. t_c is 300 μs and it is the field free time during which we observe the plasma expansion. t_a, t_b - calculations are shown later. Right: A circuit diagram representing (not the actual wiring) the system of anti-Helmholtz coils, where V_0 and V_1 are both created by the KEPCO supply and the switch represents a switch in voltage governed by the AFG3022.

The first step in eliminating the $\vec{B}$ field is estimating the inductance of the coils. By using the number of turns and some preliminary measurements, it should be $L \sim 0.01 - 0.05$ H. The resistance of the coils is $2.7\ \Omega$. The operation current while trapping atoms is ~ 6 A, which with

the given resistance corresponds to ~ 16 V output of the power supply. Thus, the power control must follow the pattern of **Figure 2.6**. The voltages are in the form they were output by the AFG, where the scale is 1 V AFG3022 signal corresponds to -3.6 V KEPCO output.

The RL circuit equation for the circuit in **Figure 2.6** is solved to determine t_a and t_b. First we determine t_b, time to reach the operational current from zero current if we apply $V_3 = +36$ V to the MOT anti-Helmlotz coils, in terms of the inductance of the coils L:

$$i_b(t) = \frac{V_3}{R}(1 - e^{\frac{-tR}{L}}) \tag{2.5}$$

$$i_b(t_b) = 6\text{A} = \frac{V_3}{R}(1 - e^{\frac{-tR}{L}}) \tag{2.6}$$

$$t_b = \frac{-\ln(1 - \frac{6R}{36})L}{R} \tag{2.7}$$

$$t_b = 0.596L/R \tag{2.8}$$

Now we complete the calculations for t_a, the time it takes to reach zero from the operational current, where we are switching from $V_1 = +16$ V to $V_2 = -36$ V applied to the MOT anti-Helmlotz coils:

$$i_a(t) = \frac{V_2 + (V_1 - V_2)e^{-tR/L}}{R} \tag{2.9}$$

$$i_a(t_a) = 0\text{A} = \frac{V_2 + (V_1 - V_2)e^{-tR/L}}{R} \tag{2.10}$$

$$t_a = -\ln\left(\frac{36}{52}\right)\frac{L}{R} \tag{2.11}$$

$$t_a = 0.367L/R \tag{2.12}$$

First we notice that the ratio $\frac{t_b}{t_a} \sim 1.6$ and so the graph in **Figure 2.6** is not to scale. We started determining the exact waveform needed to control the current by using these calculated estimates of t_a, t_b and our estimates of the inductance. These were only estimates, though, which we tested by finding the actual current in the wires during t_c while using waveforms with different t_a, t_b values. The time intervals that eliminated and restored the current most efficiently were: $t_a = 3.25$ ms and $t_b = 5$ ms. This suggests inductance of the wires of 0.024 H, which is within the range of estimated inductance and thus agrees with our general prediction. The ratio of the time intervals

is $\frac{t_b}{t_a} \sim 1.54$, which upon consideration of systematic errors also agrees with our calculations. The waveform using these t_a, t_b values gives currents of $< |200| \ \mathrm{mA}$ in the wires at all times during t_c, which is important to ensure we are observing natural, undisturbed expansion of the UNP. Screenshots of the oscilloscope displaying the current in the coils, the output of the AFG3022, and the KEPCO BOP is included in the Appendix. Also included in the **Appendix** is the waveform information as it was written in the ArbExpress software.

Chapter 3

Determining the Expansion velocity of a Rb UNP

3.1 Results, Discussion, and Limitations

As mentioned in the previous chapter, we use ion TOF spectra acquired by use of the MCP to infer the spatial evolution of the plasma over time. We collect these spatial distributions of ions at different times after the plasma creation in the range from $0.5\ \mu$s to $7 - 35\ \mu$s, depending on the initial conditions. We discussed earlier the limitations on the size of the atom posed by the MOT as well as some heating and cooling processes occurring in UNPs.

The ion TOF is the only observation method this setup has for the plasma. Thus, we are limited in the amount of information we can get from the UNP. Nevertheless, the data we have acquired is very promising and indicates that this experimental setup can be used as a method for studying the UNPs.

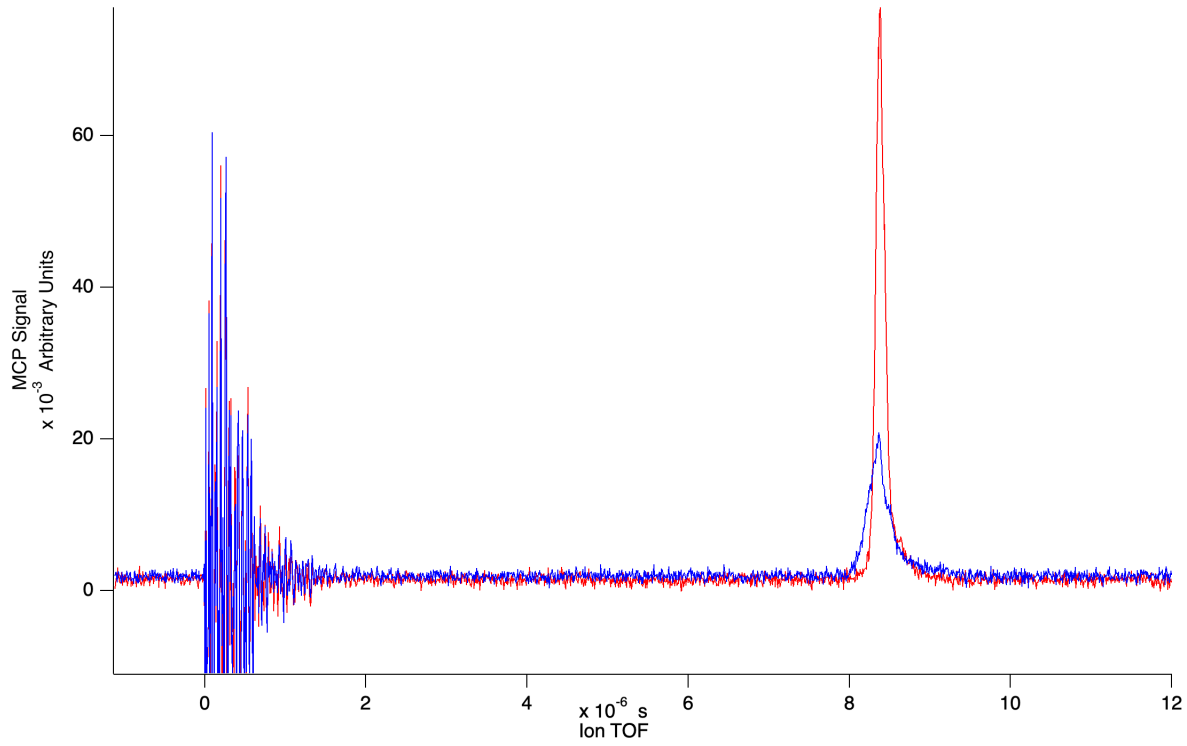

Figure 3.1: An ion TOF spectra, Red: $T_{e,i} = 1K$ with $1\mu s$ delay, Blue: $T_{e,i} = 10$ K with 16 μs. The noise part of the graph on the left side corresponds to the stripping of electrons from the plasma as that movement disturbs the detector. We can see the blue graph is wider than the red, illustrating the plasma size differences at different times after plasma creation. The relative sizes are different mostly due to the initial conditions - plasma in the blue graph was created from a smaller atom cloud.

The data is collected by means of an oscilloscope that receives information from the MCP and averages it. The averaging rate and number of datapoints per average can be adjusted, but for this experiment these were set to: 32 datapoints collected at 20 Hz. Once the data is available the data is transferred to a PC. Typical ion TOF spectra acquired in our experiment look like the ones shown in **Figure 3.1**. These show the relative amount of the ions arriving at the MCP over time after the bias field from the field meshes is applied to the system.

The ion TOF spectra are then converted to a graph of number of ions arriving from a certain position in the trap. We find these position using kinematic equations where we are assuming that

the acceleration of the ions is given by:

$$F = ma \tag{3.1}$$

$$a = \frac{F}{m} = \frac{qE}{m} = \frac{qV/d}{m} = \frac{qV}{md} \tag{3.2}$$

$$a = \frac{eV}{Am_p d} \tag{3.3}$$

where e is the charge of an electron, $V = 84.9$ V (the HV pulse), $A = 85$, m_p is the proton mass (so that $m = Am_p$), and d is the distance between the meshes $d = 18$ mm. After the ions leave the space in between the meshes, they travel at a constant velocity a distance $l = 58$ mm to the MCP, where they are detected.

This is done using Igor Pro data analysis routines written by Prof. Tate. Many of the acquired graphs do not have a peak centred at zero. There are several factors that could be contributing to this shift. The more likely reason is that the cloud itself is not centred in the middle between the field meshes. The other reason is systematic error, such as uneven bias field or remaining background field swaying the path of a portion of the ions away from (or towards) the MCP.

Despite the shifted position, most of the graphs we have collected are quite symmetric and even before analysing, we see how they have a rather Gaussian shape. Some of the transformed graphs are shown in **Figure 3.2**. Of course, there are limitations to the method of finding these positions. Many of the assumptions in the calculations of the position from the time of flight are idealised, e.g. straight paths with no collisions or no initial velocity.

Once these positions are computed, the data can be analysed for trends. We have been assuming the plasma ion distribution is Gaussian, following the theory of UNPs. Thus, we use a fitting routine (on Igor Pro) to find the Gaussian distribution for every data point, i.e. one per given initial electron temperature and bias field delay. Some example fits are included here too, see **Figure 3.3** .

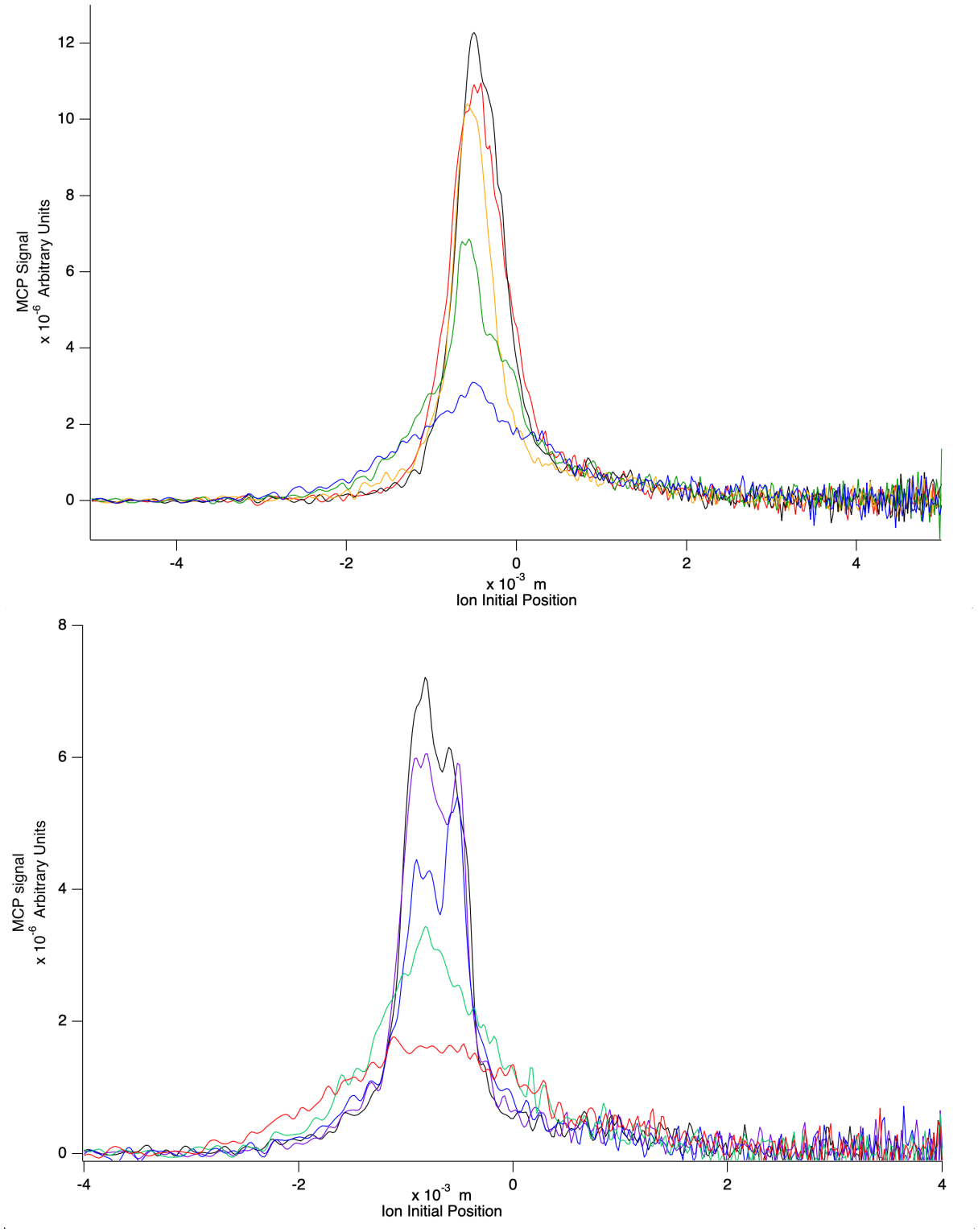

Figure 3.2: Graphs of ion distributions at different times for a plasma with TOP: $T_{e,i} = 10$ K. Red:1 μs, Black: 3 μs, Orange: 6 μs, Green: 10 μs, Blue: 16 μs. BOTTOM: $T_{e,i} = 30$ K. Red:10 μs, Green: 6 μs, Blue: 3 μs, Purple: 2 μs, Black: 1 μs. We can see the expansion of the plasma over time as well as the fact that the cloud was not centred in the middle of the trap. The second set of data exhibits much less Guassian shapes. Rather, it would seem at shorter delays that the shape is a combination of multiple Guassians.

The Gaussians represent the spatial distribution of the ions and thus σ, the characteristic width of a Gaussian distribution, is a measure of how wide the plasma is at the particular delay. Thus, we expect that graphing σ^2 over t^2 should give us a quantity related to the velocity of the plasma expansion, because we can see σ as the distance traveled and the delay as the time interval in which the distance was travelled. In particular, we expect the characteristic width of the Gaussian at a given delay to be given by:

$$\sigma^2 = v_0^2 t^2 + \sigma_0 \tag{3.4}$$

where σ_0 is the initial characteristic width of the plasma at $t = 0$. Thus, the graph of σ^2 over t^2 should have a slope corresponding to v_0^2 and an intercept corresponding to σ_0. The units of σ^2 are 10^{-6} m and units of t^2 are 10^{-12} s^2, and thus the units of v_0^2 are 10^6 $\mathrm{m}^2\mathrm{s}^{-2}$. That is, if we want the value of v_0^2 in $\mathrm{m}^2\mathrm{s}^{-2}$ we need to multiply the slope by 10^{-6}. Now, recalling **Equation 1.3** we note that:

$$v_0^2 = \frac{k_b(T_{e,0} - T_{i,0})}{m_{ion}}. \tag{3.5}$$

However, the initial temperature of the ions $T_{i,0}$ is negligible compared to that of electrons, $T_{e,0}$. Using this fact and **Equation 3.4** we can conclude that:

$$T_{e,0} = v_0^2 \frac{m_{ion}}{k_b} = \frac{\sigma^2}{t^2} 10^{-6} \frac{85 \times 1.67 \times 10^{-27}}{1.38 \times 10^{-23}} = \frac{\sigma^2}{t^2} \frac{1}{100}. \tag{3.6}$$

This is an important observation as therefore we can check whether we are collecting data that agrees with predictions by seeing whether the recorded slopes correspond to the temperatures we set our ionising laser to. That is, whether $T_{e,0}$ found matches $T_{e,i}$ set on the laser. In this way we see can further test our setup. The resulting graphs of σ^2 over t^2 for all initial conditions studied are in **Figure 3.4** and **3.5**.

We notice immediately that the graphs are not linear for lower $T_{e,i}$ and shorter delays. However, we expect these graphs to be linear as the velocity of expansion should be constant. The non-linearity is less pronounced for higher $T_{e,i}$ and later in the expansion. In addition, the linear portions of the slopes past the non-linear portion have a slope corresponding to higher $T_{e,0}$ then what the laser was set to ($T_{e,i}$). The most likely explanation for this non-linearity is three-body recombination. As discussed in **Chapter 1**, TBR creates hot electrons, which explains the steeper

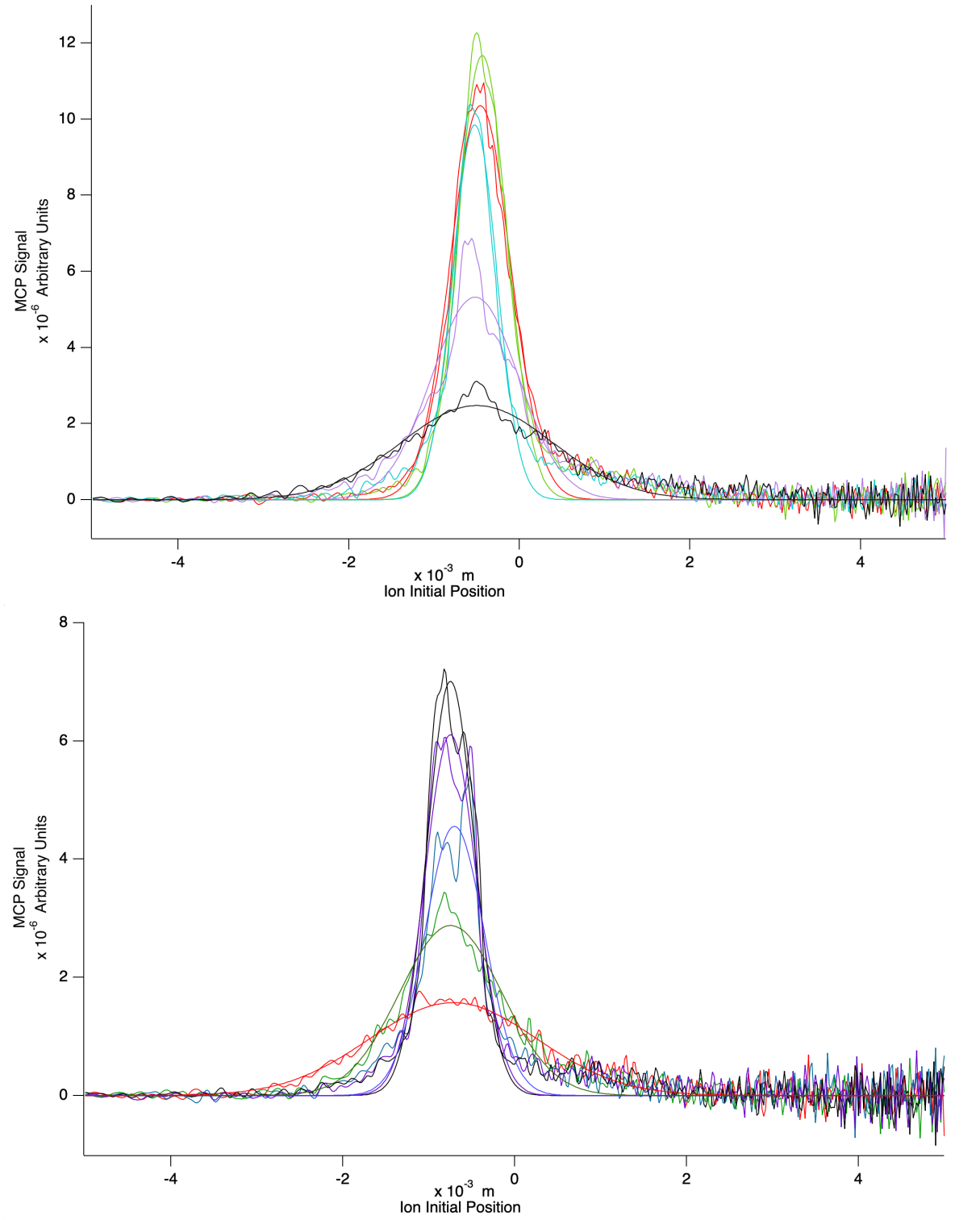

Figure 3.3: Graphs of ion distributions and their Gaussian fits for different time intervals between plasma creation and application of HV pulse to the field meshes for a plasma with TOP: $T_{e,i} = 10$K. Red:1 μs, Green: 3 μs, Blue: 6 μs, Purple: 10 μs,Black: 16 μs. BOTTOM: $T_{e,i} = 30$ K. Red:10 μs, Green: 6 μs, Blue: 3 μs, Purple: 2 μs, Black: 1 μs. We can see the expansion of the plasma as the broadening of the Gaussians over time.

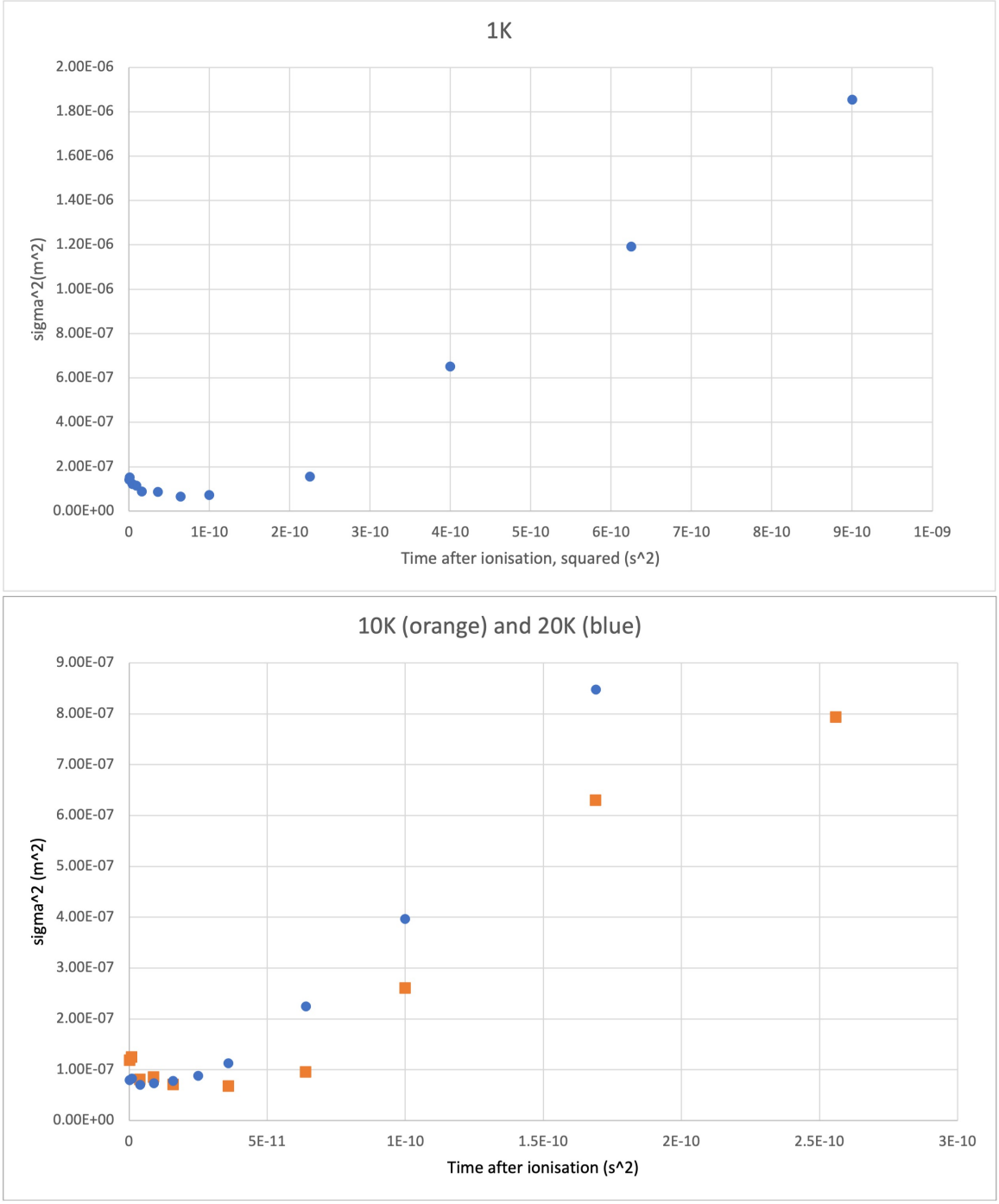

Figure 3.4: Graphs of the characteristic width of the fitted Gaussian squared over time elapsed from plasma creation squared for TOP: 1 K, BOTTOM: 10 and 20 K. We see that the graphs are more linear at later times and higher initial electron temperatures. The slopes of these graphs follow the relationship described in **Equation 3.6**.

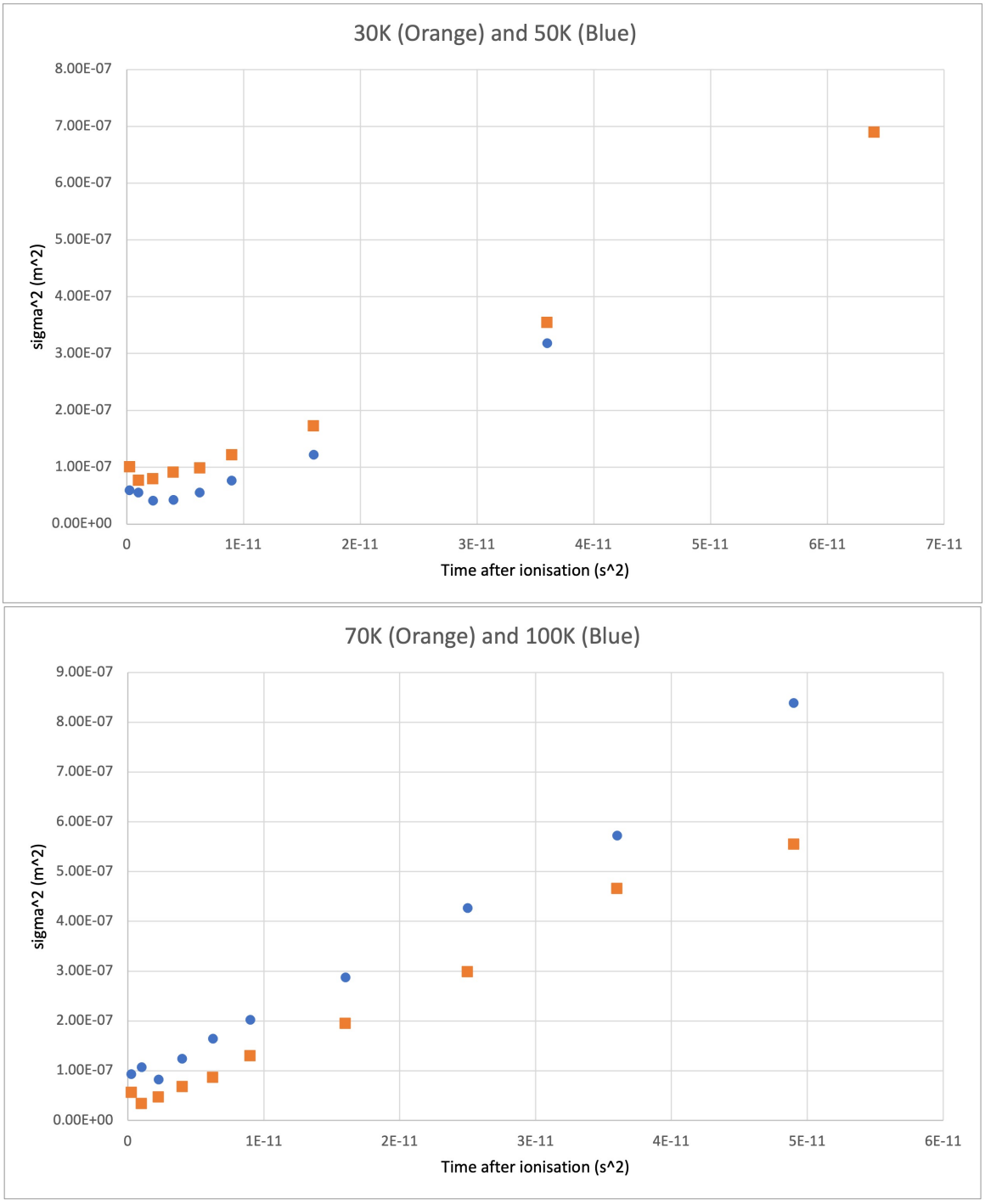

Figure 3.5: Graphs of the characteristic width of the fitted Gaussian squared over time elapsed from plasma creation squared for TOP: 30 and 50 K, BOTTOM: 70 and 100 K. We see that the graphs are more linear at later times and higher initial electron temperatures. The slopes of these graphs follow the relationship described in **Equation 3.6**.

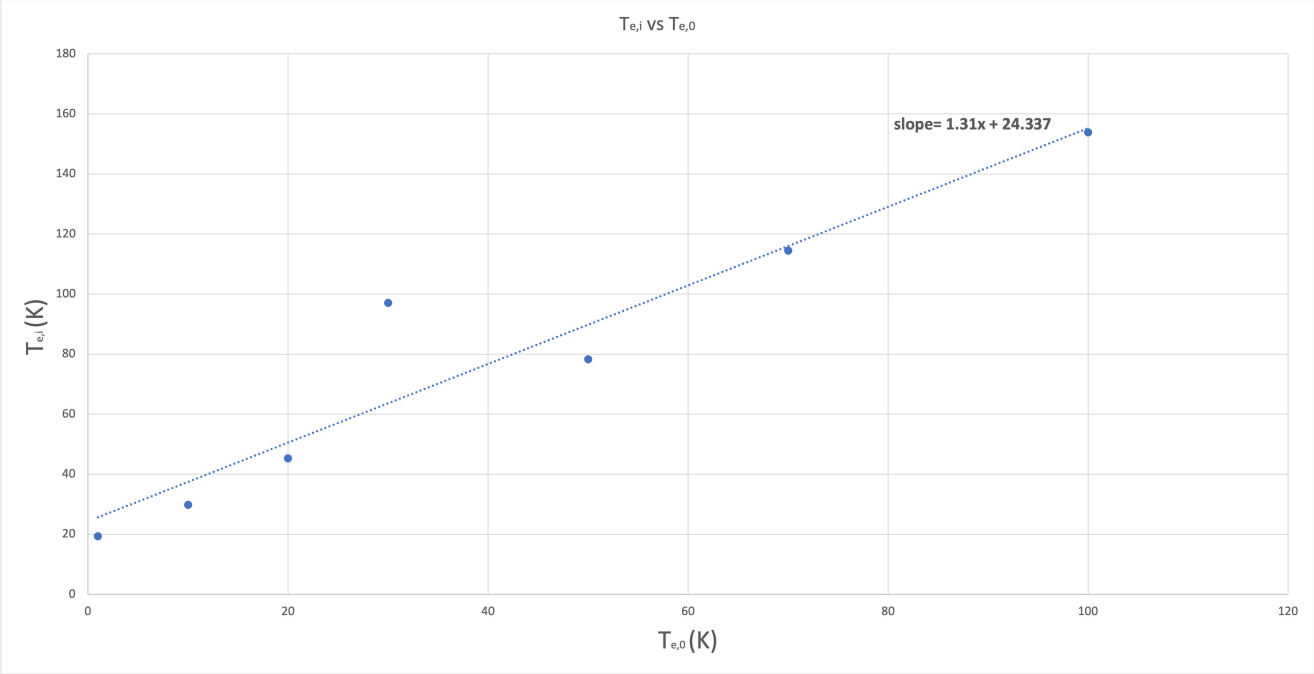

Figure 3.6: Graph showing the relationship between the initial electron temperature set using the dial on the ionising Littman laser,$T_{e,i}$, and the temperature acquired from the ion TOF spectra, $T_{e,0}$. We notice the slope is steeper than 1 and that the intercept is not at 0. This can be attributed to method limitations and some natural processes (such as TBR).

slopes in the linear portion of the graph. In addition, by combining a portion of the electrons with ions, the electron pressure inside the plasma decreases and thus temporarily slows the expansion. Though this explanation fits the observed trend, we have not conducted experiments to confirm it. It is possible this non-linearity is a result of a limitation of our setup. For example, the data is skewed for plasmas larger than the field meshes separation. The trace magnetic field could also affect the expansion by confining the atoms to the middle of the trap for a longer period than we accounted for. We graph the relationship between the temperature set on the ionising pulse laser $T_{e,i}$ and the one we get from the slopes of the graphs of the ion TOF spectra in **Figure 3.4**, $T_{e,0}$.

In an ideal situation where we detect the plasma expansion exactly and the initial conditions are known exactly, we expect the slope of **Figure 3.6** to be 1 and the zero intercept to be at 0. Even though we do not see this be met by our graph, the monotonic increase is a very promising result. In combination with the distributions pretty well fit by Gaussians we see that this experimental procedure definitely allows us to observe the plasma growth as we would expect it to. There are some imperfections that we have yet to address. Especially figuring out the effect of the

remaining magnetic field and ascertaining the origin of the non-linearity. We assume that if the non-linearities source was determined and limited the slopes of the graphs in **Figure 3.4** would give us the correct temperatures.

Considering the results obtained and the limitations of this approach, further investigations could be conducted to ascertain the origin of the non-linearity. This could be done by conducting experiments while varying different aspects of the initial conditions. For example, controlling the cloud's density, varying the bias field strength, or trying to further eliminate the background magnetic filed are all good candidates. All of these can lead to disturbances in the plasma or to an expansion that would not be reliably detectable.

If we achieve higher stability and accuracy of measurement using this experimental method, we could study the plasma behaviour in different situations (e.g. adding cold Rydberg atoms by using another laser) and reliably determine the expansion velocity and temperature of the electrons.

Chapter 4

Conclusion

UNPs have been around since 1999, but their potential has still not been fully exploited. We can achieve more strongly coupled regimes, find more accurate models for spatial and temporal behaviour, and maybe observe new behaviours altogether. This thesis is only a small step in the direction that Professor Tate's laboratory is heading, which is only one of the directions current plasma research is diverging towards.

In particular, in this thesis we managed to install a tapered amplifier to the cooling and repump lasers and increased the trapping efficiency of our MOT fourfold. We also suppressed the induced magnetic field in the trap during the experiment to minimal amounts. All of these improvements were done in order to increase our ability to precisely study the undisturbed spatial evolution of an ultra-cold Rubidium plasma.

Though there are limitations to studying the spatial evolution of UNPs using ion TOF spectra, it is also a very promising method. We are hopeful that we will be able to soon determine the origin of or eliminate the non-linearity observed at low initial electron temperatures early in the plasma lifetime, as discussed in the last chapter. Though there is still a lot of ground to cover in this direction, once this is accomplished, the goal of the Tate laboratory can be achieved - to again seed the plasma with cold Rydberg atoms in order to combat TBR and hopefully create a strongly coupled ultra-cold plasma.

Chapter 5

Appendix

5.1 Waveform Information - ArbExpress

The settings/properties of the waveform as it was written inArbExpress are as follows:

$range(0, 3.25ms)$

5

$range(3.25ms, 3.55ms)$

0

$range(3.55ms, 8.55ms)$

-5

$range(8.25ms, 15ms)$

-2.2

This is the form in which the waveform is sent to the AFG3022 via an USB cable. Once uploaded to the AFG3022, the voltage range must be adjusted to $V_{pp} = 20\text{V}$. The period will need to be set to 15ms, the slope to "positive", and the trigger source must be set to "external". The AFG3022 will then remain at the last given voltage (the operational voltage) until the next trigger comes.

5.2 Oscilloscope Screen - Behaviour of the Current in the Coils

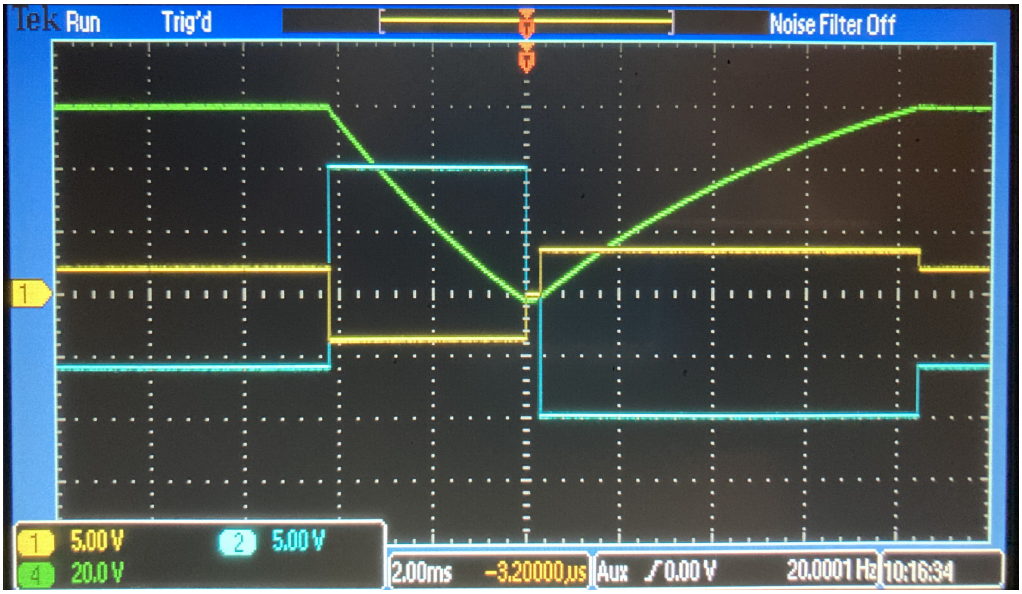

Figure 5.1: Screenshot of an oscilloscope connected to the KEPCO BOP and the AFG3022. The green curve represents the current behaviour, with the flat regions corresponding to the operational current $\sim 6\mathrm{A}$. We can see that for the experiment window of $300\mu\mathrm{s}$ it is near zero. The blue curve shows the outputs of the AFG3022. The yellow curve represents the voltage outputs of the KEPCO BOP, scaled down to -5 to $5\mathrm{V}$ range, such that $5\mathrm{V}$ corresponds to $36\mathrm{V}$.

Bibliography

[1] T. C. Killian, S. Kulin, S. D. Bergeson, L. A. Orozco, C. Orzel, and S. L. Rolston. Creation of an ultracold neutral plasma. *Physical Review Letters*, 83(23):4776–4779, December 1999.

[2] S.L. Rolston. Ultracold neutral plasmas. *Physics*, 1:2, 2008.

[3] E. V. Crockett, R. C. Newell, F. Robicheaux, and D. A. Tate. Heating and cooling of electrons in an ultracold neutral plasma using rydberg atoms. *Phys. Rev. A*, 98, October 2018.

[4] T.C. Kilian. Ultracold neutral plasmas. *Science*, 316:705–708, May 2007.

[5] E. J. Catanzaro, T. J. Murphy, E. L. Garner, and W. R. Shields. Absolute isotopic abundance ratio and atomic weight of terrestrial rubidium. *Journal of research of the National Bureau of Standards. Section A, Physics and chemistry*, 1969.

[6] S. Hamaguchi, R. T. Farouki, and D. H. E. Dubin. Triple point of yukawa systems. *Physical Review E*, 56:4671–4682, October 1997.

[7] P. Gupta, S. Laha, C. E. Simien, H. Gao, J. Castro, T. C. Killian, and T. Pohl. Electron-temperature evolution in expanding ultracold neutral plasmas. *Physical Review Letters*, 99:075005, August 2007.

[8] Craig Witte Wei-Ting Chen and Jacob L. Roberts. Observation of a strong-coupling effect on electron-ion collisions in ultracold plasmas. *PHYSICAL REVIEW E*, 96, July 2017.

[9] P. McQuillena, T. Strickler, T. Langin, and T. C. Killian. Ion temperature evolution in an ultracold neutral plasma. *Physics of Plasmas*, 22, January 2015.

[10] NobelPrize.org. The nobel prize in physics 1997.

[11] Yin Li. *Expansion of an ultracold neutral plasma*. PhD thesis, Colby College, 2019.

[12] Gabriel T. Forest, Yin Li, Edwin D. Ward, Anne L. Goodsell, and Duncan A. Tate. Expansion of an ultracold rydberg plasma. *Phys. Rev. A*, April 2018.

[13] S. Kulin, T.C. Kilian, S.D. Bergeson, and S.L. Rolston. Plasma oscillations and expansion of an ultracold neutral plasma. *Physical Review Letters*, 85:318–321, June 2000.

[14] Michael G. Littman and Harold J. Metcalf. Spectrally narrow pulsed dye laser without beam expander. *Applied Optics*, 17, 1978.

[15] D. B. Branden, T. Juhasz, T. Mahlokozera, C. Vesa, R. O. Wilson, M. Zheng, A. Kortyna, and D. A. Tate. Radiative lifetime measurements of rubidium rydberg states. *Journal of Physics B: Atomic and Molecular Physics*, 43(015002), December 2009.

[16] Wajeha Daim, Enas Al-Robayi, Rajaa Obayes, and Abdul Sada. Spectroscopic study of fluorescence coumarin 480 dye for solution with polymer. *Academic Research International Vol. 6(1) January 2015*, 6:37–81, January 2015.

[17] Ryan Cole. *Construction and Optimization of a Tapered Amplifier System for Applications in Ultra-Cold Plasma Research*. Honors thesis, Colby College, May 2015.